Noninvasive Vascular Cell Adhesion Molecule-1 Imaging Identifies Inflammatory Activation of Cells in Atherosclerosis

Matthias Nahrendorf, MD*; Farouc A. Jaffer, MD, PhD*; Kimberly A. Kelly, PhD; David E. Sosnovik, MD; Elena Aikawa, MD, PhD; Peter Libby, MD; Ralph Weissleder, MD, PhD

Background—Noninvasive imaging of adhesion molecules such as vascular cell adhesion molecule-1 (VCAM-1) may identify early stages of inflammation in atherosclerosis. We hypothesized that a novel, second-generation VCAM-1–targeted agent with enhanced affinity had sufficient sensitivity to enable real-time detection of VCAM-1 expression in experimental atherosclerosis in vivo, to quantify pharmacotherapy-induced reductions in VCAM-1 expression, and to identify activated cells in human plaques.

Methods and Results—In vivo phage display in apolipoprotein E–deficient mice identified a linear peptide affinity ligand, VHPKQHR, homologous to very late antigen-4, a known ligand for VCAM-1. This peptide was developed into a multivalent agent detectable by MRI and optical imaging (denoted VINP-28 for VCAM-1 internalizing nanoparticle 28, with 20 times higher affinity than previously reported for VNP). In vitro, VINP-28 targeted all cell types expressing VCAM-1. In vivo, MRI and optical imaging in apolipoprotein E–deficient mice (n=28) after injection with VINP-28 or saline revealed signal enhancement in the aortic root of mice receiving VINP-28 ($P<0.05$). VINP-28 colocalized with endothelial cells and other VCAM-1–expressing cells, eg, macrophages, and was spatially distinct compared with untargeted control nanoparticles. Atheromata of atorvastatin-treated mice showed reduced VINP-28 deposition and VCAM-1 expression. VINP-28 enhanced early lesions in juvenile mice and resected human carotid artery plaques.

Conclusions—VINP-28 allows noninvasive imaging of VCAM-1–expressing endothelial cells and macrophages in atherosclerosis and spatial monitoring of anti–VCAM-1 pharmacotherapy in vivo and identifies inflammatory cells in human atheromata. This clinically translatable agent could noninvasively detect inflammation in early, subclinical atherosclerosis. **(*Circulation*. 2006;114:1504-1511.)**

Key Words: atherosclerosis ■ cell adhesion molecules ■ imaging ■ inflammation ■ magnetic resonance imaging

Despite advances in cardiovascular care, the prevalence of atherosclerosis and its complications, myocardial infarction and stroke, is increasing worldwide.[1] Current noninvasive tools to assess atherosclerosis and effects of treatments rely almost entirely on structural, anatomic features of lesions. Noninvasive molecular imaging of atherosclerosis[2–5] could enable a novel biologically based approach beyond anatomy to identify vulnerable patients and to evaluate the effects of interventions, including emerging therapies. For example, inflammation appears to drive many aspects of atherogenesis and its clinical complications.[6] However, current imaging modalities disclose minimal information about this key biological process.

Clinical Perspective p 1511

Vascular cell adhesion molecule-1 (VCAM-1) (CD106), an immunoglobulin superfamily glycoprotein (100 to 110 kDa) expressed on activated endothelial cells, macrophages, and smooth muscle cells (SMCs),[7–9] participates in the inflammatory initiation and progression of atherosclerotic plaques.[6,8,10–12] VCAM-1 mediates adhesion of leukocytes to endothelial cells and facilitates their transmigration to the nascent atheromata. Furthermore, genetically modified mice with impaired VCAM-1 function have reduced atherosclerotic lesion formation.[13] Treatment with HMG-CoA reductase inhibitors[14] or angiotensin receptor blockers[15] reduces VCAM-1 expression in experimental atherosclerosis.

Received February 2, 2006; de novo received June 16, 2006; accepted July 31, 2006.

From the Center for Molecular Imaging Research (M.N., F.A.J., K.A.K., D.E.S., E.A., R.W.) and Cardiology Division, Department of Medicine (F.A.J., D.E.S.), Massachusetts General Hospital; Cardiovascular Division, Department of Medicine, Brigham and Women's Hospital (P.L.); and Donald W. Reynolds Cardiovascular Clinical Research Center, Harvard Medical School (M.N., F.A.J., K.A.K., E.A., P.L., R.W.), Boston, Mass.

Guest Editor for this article was John F. Keaney, Jr, MD.

The online-only Data Supplement is available at http://circ.ahajournals.org/cgi/content/full/CIRCULATIONAHA.106.646380/DC1.

*The first 2 authors contributed equally to this work.

Correspondence to Farouc Jaffer, MD, PhD, or Ralph Weissleder, MD, PhD, MGH-CMIR, 149 13th St, Room 5406, Charlestown, MA 02129. E-mail fjaffer@partners.org or Weissleder@helix.mgh.harvard.edu

Circulation **is available at http://www.circulationaha.org** **DOI: 10.1161/CIRCULATIONAHA.106.646380**

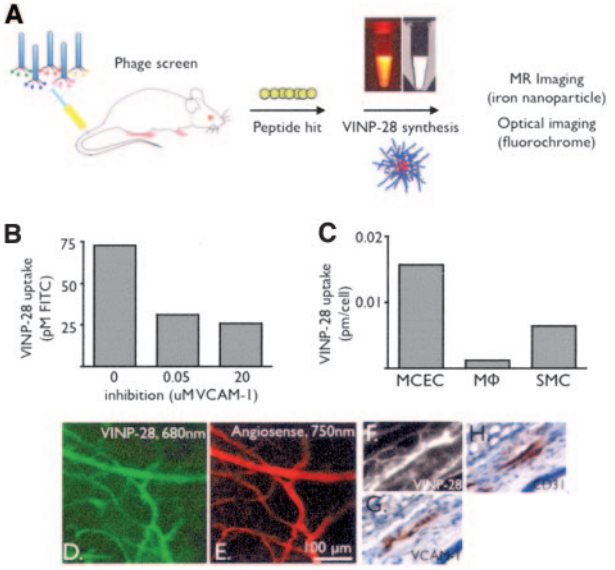

Figure 1. Peptide discovery and in vitro probe validation. A, Experimental flow scheme. In vivo phage display was performed in apoE$^{-/-}$ mice. The discovered peptide was attached to an NP, which facilitated MR and optical imaging. Eppendorf tubes symbolize optical (left) and MR (right) imaging. B, Preincubation of VINP-28 with soluble VCAM-1 results in substantially reduced uptake into cultured mouse endothelial cells, thereby affirming the specificity of VINP-28 for VCAM-1. Probe uptake was assessed by immunoassay for FITC, which is present on the targeting peptide of VINP-28. C, Analysis of VINP-28 uptake into different mouse cell types by FITC immunoassay. The probe is taken up primarily by endothelial cells but also to some extent by murine peritoneal macrophages (MΦ) and mouse aortic SMCs. D, E, Intravital multichannel laser microscopy of a mouse ear after induction of inflammation by TNF-α injection shows uptake of VINP-28 into VCAM-1–expressing cells (D, Cy5.5 channel, VINP-28; E, AF750 channel, intravascular imaging agent). F–H, Adjacent sections of fluorescent microscopy (F) and immunohistochemical staining for VCAM-1 (G) and endothelium (H; CD31) demonstrate VINP-28 uptake into activated endothelium (magnification ×200). MCEC indicates murine cardiac endothelial cells.

To image VCAM-1 expression in vivo, we had previously developed magnetic nanoparticles (MNPs) derivatized with cyclic VCAM-1–targeted peptide sequences.[16] Although this approach seemed successful in preliminary feasibility experiments as judged by ex vivo imaging of excised aortas, synthesis of imaging agents with sufficient affinity for reliable high-resolution in vivo MR imaging proved challenging. To overcome this limitation, we developed second-generation VCAM-1–targeted nanoparticles (NPs) that undergo internalization and trapping in cells that express VCAM-1, resulting in higher signal amplification than prior agents. Identification of a linear peptide sequence through in vivo phage screens enabled the development of this agent, which is made up of the peptide attached in highly multivalent fashion to magnetofluorescent NPs to yield VINP-28 (for VCAM-1 internalizing NP; Figure 1A). Cell-based assays revealed a 20-fold-higher cellular internalization of VINP-28 than previous preparations.

The present study tested the hypotheses that VINP-28 could (1) noninvasively and quantitatively image VCAM-1 expression in vivo in atherosclerosis; (2) noninvasively assess pharmacologically mediated reductions in VCAM-1; (3) facilitate imaging of early murine atherosclerosis; and (4) detect VCAM-1–expressing cells in human atheromata.

Methods

Materials; experiments investigating uptake of VINP-28 into cultured endothelial cells, macrophages, and SMCs; fluorescence reflectance imaging of resected aortas; histopathological analysis; immunoblotting; and serum cholesterol measurements are described in the online-only Data Supplement.

Nanoparticles

The MNP used in this study was a monocrystalline MNP consisting of a 3-nm core, an overall size of 38 nm, and an R2 of 62 $mM^{-1}s^{-1}$ that had an average of 62 primary amines available for conjugation.[17] Further details and peptide synthesis and conjugation are available in the online-only Data Supplement. An additional control NP (CLIO-AF750) was similar to CLIO-Cy5.5 (excitation/emission, 673/694 nm) except for containing a spectrally distinct fluorochrome (excitation/emission, 752/779 nm).

In Vivo Phage Display for Target Identification

A linear VCAM-1–targeting peptide was identified via in vivo phage display in apolipoprotein E–deficient (apoE$^{-/-}$) mice.[18] Briefly, an M13 phage library (2×10^9 individual clones) consisting of randomized linear peptides of 7 amino acids (New England Biolab, Beverly, Mass) was injected into the tail vein of cholesterol-fed apoE$^{-/-}$ mice. Internalized phages were retrieved from dissected aortic plaques and then reinjected into subsequent mice for a total of 3 rounds of positive selection. Recovered phages were plated and individual clones sequenced. The peptide sequence VHPKQHR represented >10% of the library. By BLAST search, the peptide was noted to be homologous to the very late antigen-4, a known ligand of VCAM-1,[6] and was thus chosen for specificity testing and subsequent probe synthesis.

Intravital Microscopy of VCAM-1 Expression in Tumor Necrosis Factor-α–Induced Ear Inflammation

C57BL/6 mice (n=3) were injected subcutaneously in the right ear with tumor necrosis factor (TNF)-α (5 ng in 50 μL normal saline, R&D Systems, Minneapolis, Minn) as described previously.[16] Animals were injected intravenously with 5 nmol/L fluorochrome of VINP-28, as well as an intravascular imaging agent (Angiosense-750, VisEn, Woburn, Mass). Intravital microscopy is described in detail in the online-only Data Supplement.

Imaging of Atherosclerotic Mice

A total of 67 mice were used in this study (imaging experiments: 28 apoE$^{-/-}$ mice, 32 weeks of age; 3 apoE$^{-/-}$ mice, 9 weeks of age; 13 C57BL6 mice; phage display, feasibility, dose-finding studies, and Western blot: 23 apoE$^{-/-}$ mice). ApoE$^{-/-}$ mice received a high-cholesterol diet (HCD; Harlan Teklad, Madison, Wis; 0.2% total cholesterol) for 22 weeks. All animals received VINP-28 or control NP intravenous injections (30 mg Fe/kg) 48 hours before imaging. Three experimental groups were investigated. In the validation trial, 15 mice were injected with VINP-28, 2 mice were coinjected with VINP-28 and an underivatized control NP (CLIO-AF750), and 3 mice were injected with saline. In the statin treatment group, 8 mice were randomized to receive 8 weeks of HCD enriched with 0.01% wt/wt of atorvastatin.[19] In the early atherosclerosis group, 3 apoE$^{-/-}$ mice were imaged at the 9 weeks of age after 2 weeks of an HCD. The institutional subcommittee on research animal care approved all animal studies.

MRI Studies

In vivo MRI studies were performed on a 9.4-T horizontal-bore scanner (Bruker Biospec, Billerica, Mass). Bright-blood cine images

Comparison of In Vivo and In Vitro Phage Displays

Type	Target	Results	Examples of Hits	Imaging Agents
In vivo screen	Plaques of apoE$^{-/-}$ mouse	46/87 homologous	**VHP**KQHR	VINP-28
		41/87 nonhomologous	**TASN**NNS	
			TISNKSQ	
			TYSNSYP	
In vitro screen	MCEC	28/71 homologous	**VHS**PNKK	VNP[16]
		43/71 nonhomologous	RQ**PLP**TQ	
			PLPTQVR	
			NIR**PLP**M	

A total of 158 peptide sequences were investigated (87 from in vivo screen, 71 from in vitro screen). A comparison of the screens showed that 47% of peptide motifs were homologous. As an example for homology, the VCAM-1–targeting affinity ligand is shown. Consensus sequences are shown in bold. In the nonmatching motifs, an example family from 1 screen is shown.

were obtained with ECG and respiratory gating (SA Instruments, Stony Brook, NY) using a gradient-echo FLASH sequence and a dedicated mouse cardiac surface coil. A short-axis slice through the aortic root was identified. Care was taken to ensure that all 3 aortic valve cusps were clearly visualized to provide fiducial landmarks for coregistration with subsequent MR images and with images from other modalities. Imaging parameters and image analysis are described in the online-only Data Supplement.

Fluorescence Microscopy

The cellular distribution of VINP-28 and control NPs in atheroma was assessed with multichannel fluorescent microscopy. Sections were imaged with an upright epifluorescent microscope (Eclipse 80i, Nikon, New York, NY) with a cooled CCD camera (Cascade, Photometrics, Tucson, Ariz) at a wavelength of 710 nm (for VINP-28) and 780 nm (for untargeted NP). Exposure times ranged from 100 to 2000 ms, depending on the channel.

Human Carotid Artery Specimens

Freshly resected carotid endarterectomy specimens were immediately placed in Dulbecco's modified Eagle's medium under sterile conditions. The specimens were incubated with either VINP-28 or buffer for 24 hours at 37°C. The T2 relaxation time was determined before and after incubation with a minispectrometer (Bruker), and fluorescence reflectance imaging was performed. Thereafter, the sections were embedded in OCT and processed for correlative fluorescence microscopy and immunohistochemistry.

Statistical Analysis

Results are expressed as mean±SD. Statistical comparisons between 2 groups were evaluated by Student *t* test and corrected by ANOVA for multiple comparisons. A value of $P<0.05$ was considered statistically significant.

The authors had full access to and take full responsibility for the integrity of the data. All authors have read and agree to the manuscript as written.

Results

VINP-28 Targets VCAM-1–Expressing Cells

Iterative in vivo phage display identified the linear peptide VHPKQHR as homologous but not identical to a peptide identified on a previous in vitro screen[16] using a disulfide-constrained library on endothelial cells (the Table). We compared the peptide sequences isolated through the in vivo screen to the previous in vitro phage display with the RELIC software (shareware) and found a 47% overlap in consensus families. Among such families, 27% were strictly confined to the in vitro screen and 26% to the in vivo screen.

The peptide sequence was synthetically extended at its amine terminal and conjugated in multivalent form (12 copies per NP) to yield VINP-28 (Figure 1A). Soluble VCAM-1 blocked endothelial uptake of VINP-28 at low concentrations (Figure 1B). Among primary murine endothelial cells, SMCs, and macrophages, VINP-28 had the highest affinity for endothelial cells, with relatively lower levels of accumulation in SMCs and macrophages, cells known to express variable

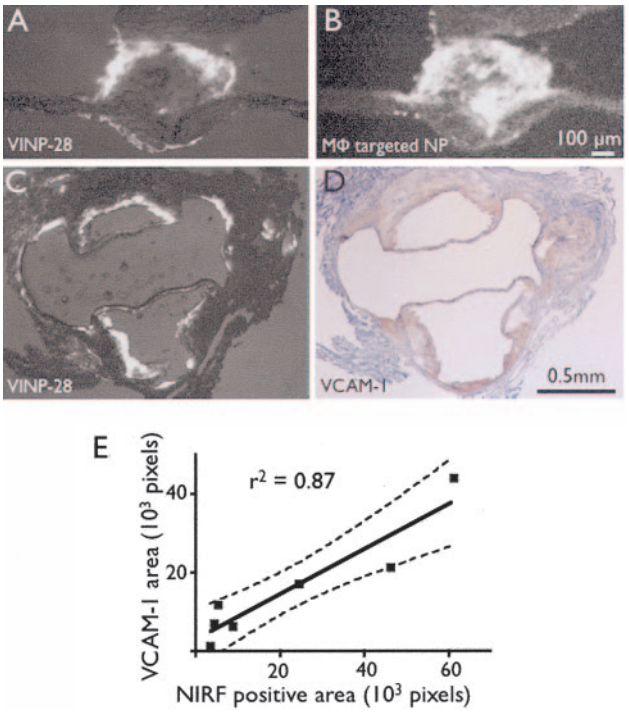

Figure 2. VINP-28 probe validation in murine atheromata. A, B, Coinjection of VINP-28 derivatized with cyanine 5.5 (excitation emission, 675/694 nm; A) and CLIO-AF750 (excitation/emission, 752/779 nm; B) into the same mouse allows a spectrally resolved control experiment demonstrating that the distribution of the VCAM-1–targeted probe is distinct from the control NP, which was derivatized with the higher-wavelength fluorochrome AF750. C, D, Colocalization of uptake of VINP-28 detected by fluorescent microscopy in the 680-nm channel (C) with VCAM-1 expression in immunohistochemistry (D). Probe uptake as assessed by NIR-positive root area and the VCAM-1–positive area by immunohistochemical studies (E) demonstrated good correlation ($r^2=0.87$, $P<0.005$; n=7).

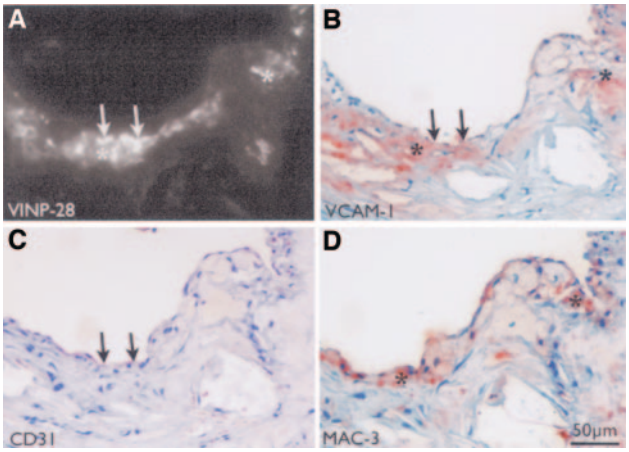

Figure 3. In vivo cellular distribution of VINP-28. A, VINP-28 distribution in murine atherosclerotic plaque assessed by fluorescent microscopy (magnification ×200, 680-nm channel) shows uptake into endothelial cells as indicated by arrows (C; CD31) and macrophages as indicated by asterisks (D; MAC-3) that express VCAM-1 (B) on adjacent sections.

levels of VCAM-1 in mice[7] (Figure 1C). A direct comparison with a first-generation version of the agent (VNP) showed a 20-fold improvement in flow cytometric signal (410.4 mean fluorescence units for VINP-28 versus 19.4 mean fluorescence units for VNP; $P<0.001$). In the inflamed ear preparation, intravital microscopy showed strong enhancement in VCAM-1–positive vascular endothelium, as defined by the coinjected intravascular dye (Figure 1D through 1H). VINP-28 was injected into C57BL/6 mice to determine blood half-life and biodistribution. The blood half-life in mice was 17.7 hours and the organ distribution 6 hours after injection was as follows (percent injected dose [ID]): liver, 2.83±0.53 ID/g; spleen, 0.82±0.19 ID/g; kidneys, 1.87±0.14 ID/g; heart, 0.90±0.18 ID/g; lungs, 0.77±0.15 ID/g; fat, 0.20±0.28 ID/g; and muscle, 0.22±0.16 ID/g.

VINP-28 Selectively Targets VCAM-1–Expressing Cells in Atheromata

We next determined whether the cellular localization of VINP-28 in atherosclerotic lesions was distinct from clinical-type control NPs that primarily target macrophages in atheromata.[20–22] Coinjection of VINP-28-Cy5.5 and NP-AF750 into the same apoE$^{-/-}$ mice revealed that VINP-28 strongly accumulated in the endothelial layer and subendothelial plaque regions (Figure 2A) and was distinct from control NPs (Figure 2B). Fluorescence microscopy of the distribution of VINP-28 correlated well with immunohistochemistry for VCAM-1 expression (Figure 2C through 2E; $r^2=0.87$, $P<0.005$; n=7). VINP-28 targeted endothelial cells and macrophages that expressed VCAM-1 (Figure 3). We determined that 94±2% of endothelial cells and 58±4% of macrophages contained VINP-28. These cells also stained positive for VCAM-1 in adjacent sections (Figure 3).

Noninvasive MR Imaging of VCAM-1 Expression

We next determined the ability of VINP-28 to assess VCAM-1 expression noninvasively in atherosclerosis. In particular, the aortic root, an expected area of atherosclerosis

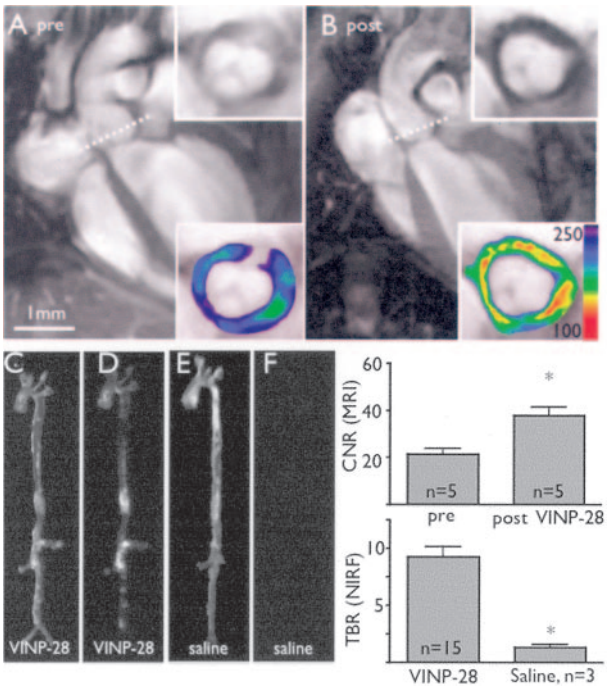

Figure 4. In vivo MR and optical imaging of VCAM-1 expression. A, MRI before injection of VINP-28. Dotted line depicts location of short-axis view (insets, lower panel with color coded signal intensity). B, Same mouse 48 hours after injection of VINP-28. A marked signal drop in the aortic root wall was noted (insets). The contrast-to-noise ratio (CNR) of the aortic wall was increased significantly after injection of the probe (mean±SD; *$P<0.05$ before vs after injection). C, E, Light images of excised aortas. D, NIRF image after VINP-28 injection demonstrates distribution of the agent to plaque-bearing segments of the aorta, whereas the aorta of the saline injected apoE$^{-/-}$ shows very little fluorescent signal (F). Both images were acquired with identical exposure times and were identically windowed. The target-to-background ratio (TBR) was significantly higher in the VINP-28 injected mice (*$P<0.05$).

in apoE$^{-/-}$ mice,[23] showed high VINP-28 uptake and change in MRI signal (Figure 4A and 4B). The contrast-to-noise ratio between the aortic wall and adjacent blood pool increased on average by 77%, driven by a decrease in signal intensity in the aortic wall ($P<0.05$; Figure 4A and 4B). The in vivo MR findings correlated with the fluorescent reflectance images of resected aortas, which showed a strong fluorescent signal from VINP-28 in aortic atheromata. The aortic root yielded a high plaque target-to-background ratio of 9.2±2.5 (>350% higher than in saline-injected apoE$^{-/-}$ mice; $P<0.05$; Figure 4C through 4F).

VINP-28 Detects Reductions in VCAM-1 Expression Produced by Statin Treatment

To determine the ability of VINP-28 to monitor pharmacotherapy for atherosclerosis, we imaged apoE$^{-/-}$ mice that consumed an atherogenic diet without or with admixed atorvastatin (Figure 5). Eight weeks of statin treatment reduced serum cholesterol moderately, as expected, in mice (HCD, 601±34 mg/dL; HCD plus atorvastatin, 506±79 mg/dL; $P<0.05$). Statin-treated mice exhibited minimal vessel wall enhancement after VINP-28 injection (blood-plaque contrast-to-noise ratio before injection, 21.4±5.5; after injec-

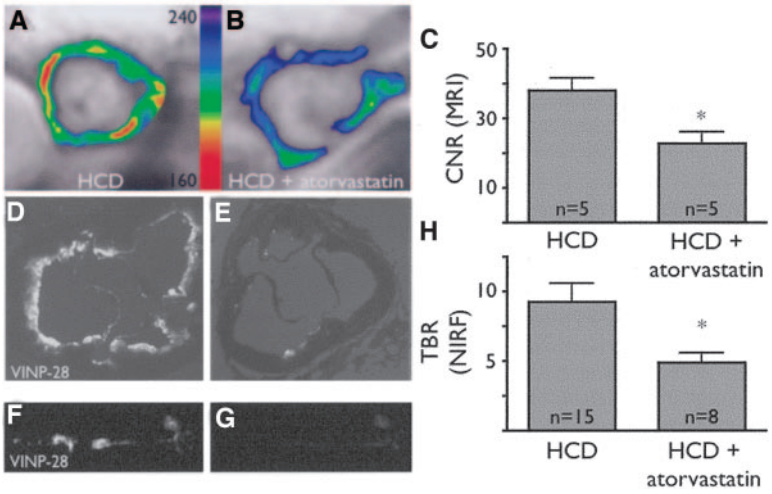

Figure 5. Noninvasive MRI assessment of VCAM-1 expression after atorvastatin administration. A, Short-axis MRI of the aortic root of an untreated apoE$^{-/-}$ mouse on an HCD after VINP-28 injection with color-coded signal intensity. B, MRI of HCD+atorvastatin apoE$^{-/-}$ mouse after VINP-28 injection. An attenuated signal drop in the aortic root wall compared with untreated mouse was noted. The red color encodes high VCAM-1 expression. C, After injection of VINP-28, the MRI contrast-to-noise ratio diminished in atorvastatin-treated mice (mean±SD; *P<0.05 vs HCD). D, E, NIR microscopy of aortic root depicted in A and B. Fluorescent signal originating from VINP-28 comprised the whole-root circumference (D), but less so in atorvastatin-treated mice (E). F, H, Fluorescent reflectance imaging of the excised aorta of an untreated (F) and atorvastatin-treated (G) mouse showed reduced NIR signal in statin-treated mice. The target-to-background ratio was reduced in aortas of treated mice (H; mean±SD; *P<0.05 treated vs untreated mice).

tion, 22.9±7.0, P=NS; Figure 5B), consistent with reduced VCAM-1 expression in the aortic root of statin-treated mice. In contrast, the plaque-blood contrast-to-noise ratio differed substantially in HCD-only mice (HCD, 37.9±3.5; HCD plus atorvastatin, 22.9±7.0; P<0.05; Figure 5A through 5C).

By fluorescent reflectance imaging, statin-treated animals had significantly less VINP-28–associated near-infrared fluorescence (NIRF) signal (Figure 5F through 5H; target-to-background ratio, 4.9±1.6 versus 9.3±3.8, P<0.05).

Fluorescence microscopy showed only slight VINP-28 uptake in aortic roots of statin-treated mice (Figure 5D and 5E). We quantified the NIRF signal in aortic root sections and normalized it by total plaque area. This index decreased significantly in statin-treated mice (HCD, 18.5±2.1; HCD plus atorvastatin, 4.1±1.8 [arbitrary units]; P<0.01), thus demonstrating that the atorvastatin-related MRI signal changes did not depend primarily on changes in lesion size. VINP-28 imaging findings in statin-treated animals correlated well with VCAM-1 reductions as measured by immunohistochemistry and immunoblotting (Figure 6).

Imaging of VCAM-1 Expression in Early Atheromata

Because arterial VCAM-1 expression increases early in atherogenesis,[6,8,10,13] it might serve as a useful target for molecular imaging of subclinical disease.[3] We therefore determined whether VINP-28–enhanced imaging could detect early atherosclerotic lesions in juvenile apoE$^{-/-}$ mice (age, 9 weeks) that consumed an HCD for only 2 weeks. Indeed, VINP-28 enhanced early atheroma in the aortic root, aortic arch, and proximal great vessels; distal carotid arteries; abdominal aorta at the level of the renal arteries; and iliac arteries (Figure 7). By reflectance imaging, the plaque target-to-background ratio was 61% higher than in saline-injected mice (P<0.05). By fluorescence microscopy, VINP-28 enhanced early lesions and colocalized with VCAM-1 in endothelial cells and macrophages (Figure 7C through 7G), as seen in older apoE$^{-/-}$ mice.

VINP-28 Identifies VCAM-1–Expressing Cells in Human Carotid Atheromata Ex Vivo

To investigate the ability of VINP-28 to target human VCAM-1 expression in atherosclerosis, the agent or saline was incubated with freshly resected human carotid endarterectomy specimens (n=2). VINP-28 induced changes in the MR signal in atheroma. After 24 hours, samples incubated with saline exhibited a T2 increase of 1.5±1 ms. In contrast, plaque sections incubated with VINP-28 demonstrated a T2 reduction of 3.8±1.7 ms (P<0.05 versus saline), consistent with VINP-28 uptake by the specimen. Fluorescence imaging showed strong plaque enhancement in VINP-28–incubated samples (Figure 8A and 8B). Microscopy revealed that

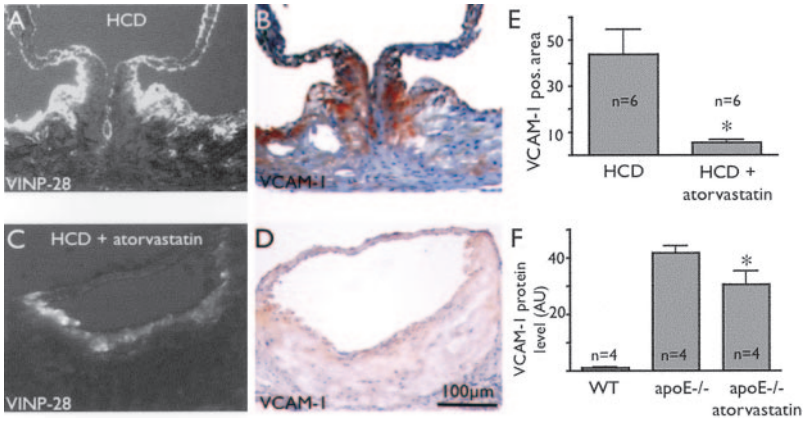

Figure 6. Assessment of atorvastatin treatment by invasive measures. A–E, Treatment with atorvastatin led to reduced probe uptake as assessed by fluorescence microscopy (A, untreated; C, treated) and a decreased immunohistochemistry staining for VCAM-1 (B, untreated; C, treated). The root area with positive immunohistochemical detection of VCAM-1 was smaller in atorvastatin-treated mice (E; *P<0.05). F, Western blotting corroborated reduced VCAM-1 expression in statin-treated mice (*P<0.05). WT indicates wild type; AU, arbitrary units.

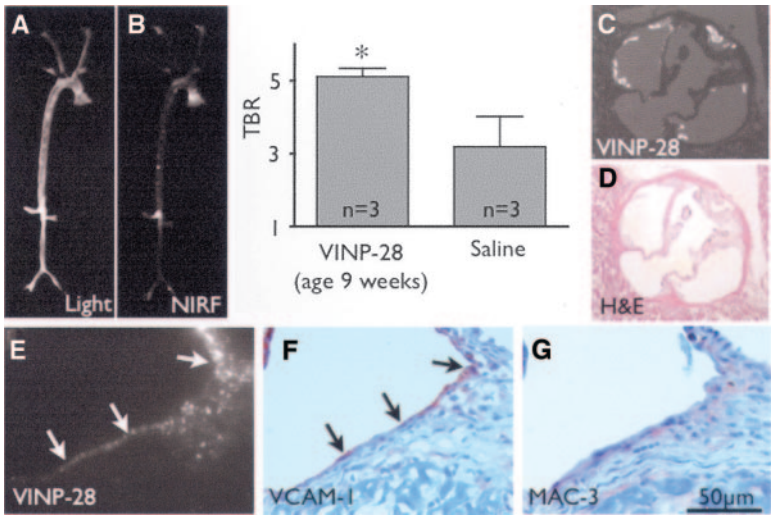

Figure 7. VINP-28–facilitated imaging of early atherosclerosis in 9-week-old apoE$^{-/-}$ mice. A, Light image of excised aorta visualizes the plaque locations. B, NIR image after VINP-28 injection facilitates imaging of early lesions in the aorta and branch vessels. The target-to-background ratio was significantly increased compared with saline-injected mice (*$P<0.05$). C, Fluorescence microscopy and hematoxylin and eosin stain (D) demonstrate uptake in early atherosclerotic lesions. E–G, Similar to mature lesions, VINP-28 colocalizes with VCAM-1–expressing endothelial cells (F; immunohistochemical detection of VCAM-1) and macrophages (G; immunohistochemical detection of macrophages).

VINP-28 colocalized with VCAM-1–expressing cells as assessed by immunohistochemistry (Figure 8C and 8D).

Discussion

Expression of the adhesion molecule VCAM-1 occurs early during atherogenesis[6,8,10] and thus may serve as a useful imaging biomarker for inflammation in atherosclerosis. Here, we demonstrate that the novel imaging agent VINP-28 allows in vivo assessment of VCAM-1 in mouse atherosclerotic plaques. The multivalent MRI agent, targeted by a peptide sequence identified via in vivo phage selection, selectively visualized both murine and human VCAM-1. VINP-28 enhanced atheroma on noninvasive MRI, allowed assessment of modulated VCAM-1 levels in response to an intervention, detected early atheromata (fatty streak–like lesions), and targeted VCAM-1–expressing cells of human carotid atherosclerotic plaques. Multimodality MRI and NIRF imaging findings correlated closely with VCAM-1 expression as disclosed by immunohistochemistry and immunoblotting. The specific agent and the generic approach used in its discovery may represent valuable tools for expanded in vivo imaging of molecular targets in atherosclerosis.

Facilitated by the fluorescent properties of NPs, we found that VINP-28 targets endothelial cells and macrophages that express VCAM-1 (Figure 3). Previous reports established the expression of VCAM-1 by these cell types.[7–9] VINP-28 also labeled macrophages and SMCs in vitro, although to a lesser degree than endothelial cells. Therefore, VINP-28 reports on the cellular content of all cells that express VCAM-1, including endothelial cells and macrophages. Because macrophages outnumber endothelial cells in inflamed atherosclerotic lesions, they may contribute considerably to MRI contrast enhancement in vivo through VCAM-1–facilitated probe uptake.

We identified the peptide affinity ligand sequence with in vivo phage display technology. Compared with a previous in vitro screen on endothelial cells, the motif overlap (47%) likely indicates specificity of those sequences for endothelial targets. Differences in the 2 screens explain the remaining nonmatching motifs; although we used only 1 cell type in the in vitro experiment (murine cardiac endothelial cells),[16] the current display exposed the phages to the in vivo milieu of atherosclerotic plaques, thus introducing more complexity with respect to pharmacokinetic barriers and additional cell types.

VINP-28 is a model magnetofluorescent NP with favorable biophysical properties. The NP contains a superparamagnetic iron oxide core and a stable, biodegradable coating that permits surface attachment of peptides. Similar preparations (with cross-linked polymer coating) have shown low toxicity in clinical trials[24] and are biodegradable.[25] VINP-28 has an R2 of 62 $mM^{-1}s^{-1}$ in aqueous solution, allowing sensitive detection by MRI. Additional factors further boosted the MRI-detectable signal: Cellular internalization of VINP-28 leads to "trapping" (active accumulation) and a relaxation switch effect, effectively increasing R2 in tissue to >250 $mM^{-1}s^{-1}$.[26] Cellular internalization and retention is a powerful biological amplification strategy that can enhance visual-

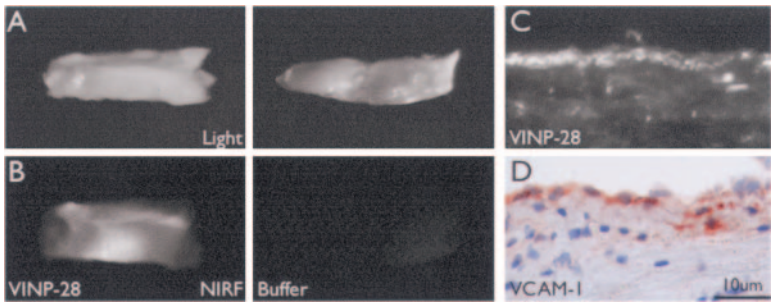

Figure 8. VINP-28 visualizes VCAM-1 in human carotid arteries ex vivo. A, Light images of human carotid specimens. B, NIR images of carotid specimens. The left specimen was incubated with VINP-28 and showed strong NIR signal. C, Fluorescence microscopy of the VINP-28–incubated section displays a signal that colocalizes with VCAM-1 expression in immunohistochemical staining of an adjacent section (D).

ization of gene expression[27] and underlies many nuclear imaging techniques. Sensitive in vitro assays[26] and in vivo imaging[28] have exploited this effect. Finally, the bright fluorescence of VINP-28 enables the direct detection by fluorescence imaging and microscopy. Although we exploited this feature to correlate the in vivo localization of the imaging agent with immunohistochemical study, it also could serve to sense distribution by intravascular fluorescence catheters[29] or tomographic detection.[30]

In vivo imaging of targeted NPs in murine arteries poses considerable technical challenges. The small size of the major vessels necessitates the acquisition of images with high spatial resolution. In addition, the rapid heartbeat and respiratory rate of the mouse demand highly accurate physiological monitoring and gating. Nevertheless, we have recently shown the feasibility of imaging targeted MNPs in the beating mouse heart.[31] Here, we chose to image the aortic root in its short axis for several reasons. First, the root develops early and consistent atherosclerotic lesions in the apoE$^{-/-}$ mouse and traditionally serves as a site for their histological quantification.[23] Second, the 3 leaflets of the aortic valve provide recognizable fiducial landmarks for consistent and reproducible positioning of the image plane. This feature allows correlation of sequential MR images with each other and coregistration of the aortic root with other imaging modalities. Finally, the anterior position of the aortic valve is well situated for imaging with a dedicated cardiac surface coil. Images of the aortic root could be obtained with this technique with high spatial resolution and excellent signal-to-noise and contrast-to-noise characteristics (Figure 4). Changes in signal intensity and blood-plaque contrast-to-noise ratio made up the principal MRI readouts in this study. However, the use of parametric techniques such as T2* maps and a recently described off-resonance technique for positive iron oxide contrast[32] might allow detection of probe accumulation with even greater sensitivity.

VCAM-1 participates in cardiovascular tissue remodeling[33] and a number of inflammatory diseases, including atherogenesis,[6,10–13] transplant rejection,[34,35] allograft arteriosclerosis,[36] asthma,[37,38] and cancer.[39,40] VCAM-1 therefore represents an attractive imaging and potential therapeutic target beyond atherosclerosis. Assessment of VCAM-1 expression by VINP-28–enhanced MRI offers a sensitive and noninvasive approach to test novel VCAM-1–targeted therapies. Its usefulness for pharmaceutical development could involve serial imaging studies that assess VCAM-1 expression before and after treatment with a novel candidate therapy. In atherosclerosis, VINP-28 can noninvasively detect statin-associated decreases in VCAM-1 expression in apoE$^{-/-}$ mice (Figure 5). Immunohistochemical studies, Western blotting, and NIRF imaging confirmed reduced VCAM-1 expression in the statin group. These findings agree with earlier histopathological studies that demonstrated a statin-associated decrease in VCAM-1 expression in atheromata of nonhuman primates,[14] rabbits,[41] and mice.[42]

Molecular imaging methods to detect atherosclerotic lesions can potentially improve diagnosis, risk stratification, and therapy of patients with atherosclerosis.[2–5] By providing a noninvasive biological readout of inflammation in atherosclerosis, VINP-28–enhanced MRI could offer complementary information to structural imaging methods. The early expression of the target molecule in the time course of the disease and the excellent avidity of VINP-28 achieved by several amplification strategies allow identification of very early stages of atherosclerosis, as demonstrated in juvenile apoE$^{-/-}$ mice. VINP-28 also enhanced VCAM-1–expressing cells in human plaques (Figure 8). On a translational level, VINP-28 may thus detect not only the presence of atherosclerotic lesions but also their degree of inflammatory activation, an important mechanism implicated in clinical complications of atherosclerosis leading to events such as myocardial infarction and stroke.[6] Early detection of inflamed plaques could identify the high-risk individual who may warrant intensive risk reduction.

Acknowledgments

We thank members of the CMIR Chemistry Core, including Drs Fred Reynolds for the conjugation of peptides, Nikolay Sergeyev for the synthesis of CLIO-CY5.5 and CLIO-AF750, and Lee Josephson for many helpful discussions. We acknowledge the CMIR Pathology Core (Vincent Lok, BS) for assistance with histology; Dr Masanori Aikawa and Manabu Minami for supplying murine aortic SMCs; Kelly Kristof, BA, and Dr Ashvin Pande for cell culture experiments; Drs Glenn LaMuraglia and Christopher Kwolek, MGH Vascular Surgery, and Matthew Spotnitz, MS, for assistance in obtaining carotid endarterectomy specimens; Dr Rainer Kohler for intravital microscopy; and Dr Guangping Dai, Martinos Center for Biomedical Imaging.

Sources of Funding

This work was supported by the Donald W. Reynolds Foundation (Drs Libby, Weissleder, Jaffer, Nahrendorf, and Aikawa), RO1-HL078641 (Dr Weissleder), ROI-HL36436 (Dr Libby), UO1-HL080731 (Dr Weissleder), and P01-AI 054904 (Dr Weissleder).

Disclosures

None.

References

1. Murray CJ, Lopez AD. Global mortality, disability, and the contribution of risk factors: Global Burden of Disease Study. *Lancet*. 1997;349:1436–1442.
2. Choudhury RP, Fuster V, Fayad ZA. Molecular, cellular and functional imaging of atherothrombosis. *Nat Rev Drug Discov*. 2004;3:913–925.
3. Jaffer FA, Libby P, Weissleder R. Molecular and cellular imaging of atherosclerosis: emerging applications. *J Am Coll Cardiol*. 2006;47:1328–1338.
4. Jaffer FA, Weissleder R. Molecular imaging in the clinical arena. *JAMA*. 2005;293:855–862.
5. Jaffer FA, Weissleder R. Seeing within: molecular imaging of the cardiovascular system. *Circ Res*. 2004;94:433–445.
6. Libby P. Inflammation in atherosclerosis. *Nature*. 2002;420:868–874.
7. Iiyama K, Hajra L, Iiyama M, Li H, DiChiara M, Medoff BD, Cybulsky MI. Patterns of vascular cell adhesion molecule-1 and intercellular adhesion molecule-1 expression in rabbit and mouse atherosclerotic lesions and at sites predisposed to lesion formation. *Circ Res*. 1999;85:199–207.
8. Li H, Cybulsky MI, Gimbrone MA Jr, Libby P. Inducible expression of vascular cell adhesion molecule-1 by vascular smooth muscle cells in vitro and within rabbit atheroma. *Am J Pathol*. 1993;143:1551–1559.
9. Libby P, Li H. Vascular cell adhesion molecule-1 and smooth muscle cell activation during atherogenesis. *J Clin Invest*. 1993;92:538–539.
10. Cybulsky MI, Gimbrone MA Jr. Endothelial expression of a mononuclear leukocyte adhesion molecule during atherogenesis. *Science*. 1991;251:788–791.
11. Nakashima Y, Raines EW, Plump AS, Breslow JL, Ross R. Upregulation of VCAM-1 and ICAM-1 at atherosclerosis-prone sites on the endothe-

lium in the ApoE-deficient mouse. *Arterioscler Thromb Vasc Biol*. 1998; 18:842–851.
12. O'Brien KD, Allen MD, McDonald TO, Chait A, Harlan JM, Fishbein D, McCarty J, Ferguson M, Hudkins K, Benjamin CD, et al. Vascular cell adhesion molecule-1 is expressed in human coronary atherosclerotic plaques. Implications for the mode of progression of advanced coronary atherosclerosis. *J Clin Invest*. 1993;92:945–951.
13. Cybulsky MI, Iiyama K, Li H, Zhu S, Chen M, Iiyama M, Davis V, Gutierrez-Ramos JC, Connelly PW, Milstone DS. A major role for VCAM-1, but not ICAM-1, in early atherosclerosis. *J Clin Invest*. 2001; 107:1255–1262.
14. Sukhova GK, Williams JK, Libby P. Statins reduce inflammation in atheroma of nonhuman primates independent of effects on serum cholesterol. *Arterioscler Thromb Vasc Biol*. 2002;22:1452–1458.
15. Candido R, Allen TJ, Lassila M, Cao Z, Thallas V, Cooper ME, Jandeleit-Dahm KA. Irbesartan but not amlodipine suppresses diabetes-associated atherosclerosis. *Circulation*. 2004;109:1536–1542.
16. Kelly KA, Allport JR, Tsourkas A, Shinde-Patil VR, Josephson L, Weissleder R. Detection of vascular adhesion molecule-1 expression using a novel multimodal nanoparticle. *Circ Res*. 2005;96:327–336.
17. Weissleder R, Kelly K, Sun EY, Shtatland T, Josephson L. Cell-specific targeting of nanoparticles by multivalent attachment of small molecules. *Nat Biotechnol*. 2005;23:1418–1423.
18. Liu C, Bhattacharjee G, Boisvert W, Dilley R, Edgington T. In vivo interrogation of the molecular display of atherosclerotic lesion surfaces. *Am J Pathol*. 2003;163:1859–1871.
19. Kleemann R, Verschuren L, de Rooij BJ, Lindeman J, de Maat MM, Szalai AJ, Princen HM, Kooistra T. Evidence for anti-inflammatory activity of statins and PPARalpha activators in human C-reactive protein transgenic mice in vivo and in cultured human hepatocytes in vitro. *Blood*. 2004;103:4188–4194.
20. Kooi ME, Cappendijk VC, Cleutjens KB, Kessels AG, Kitslaar PJ, Borgers M, Frederik PM, Daemen MJ, van Engelshoven JM. Accumulation of ultrasmall superparamagnetic particles of iron oxide in human atherosclerotic plaques can be detected by in vivo magnetic resonance imaging. *Circulation*. 2003;107:2453–2458.
21. Litovsky S, Madjid M, Zarrabi A, Casscells SW, Willerson JT, Naghavi M. Superparamagnetic iron oxide–based method for quantifying recruitment of monocytes to mouse atherosclerotic lesions in vivo: enhancement by tissue necrosis factor-alpha, interleukin-1beta, and interferon-gamma. *Circulation*. 2003;107:1545–1549.
22. Schmitz SA, Coupland SE, Gust R, Winterhalter S, Wagner S, Kresse M, Semmler W, Wolf KJ. Superparamagnetic iron oxide-enhanced MRI of atherosclerotic plaques in Watanabe hereditable hyperlipidemic rabbits. *Invest Radiol*. 2000;35:460–471.
23. Meir KS, Leitersdorf E. Atherosclerosis in the apolipoprotein-E-deficient mouse: a decade of progress. *Arterioscler Thromb Vasc Biol*. 2004;24: 1006–1014.
24. Harisinghani MG, Barentsz J, Hahn PF, Deserno WM, Tabatabaei S, van de Kaa CH, de la Rosette J, Weissleder R. Noninvasive detection of clinically occult lymph-node metastases in prostate cancer. *N Engl J Med*. 2003;348:2491–2499.
25. Shen T, Weissleder R, Papisov M, Bogdanov A Jr, Brady TJ. Monocrystalline iron oxide nanocompounds (MION): physicochemical properties. *Magn Reson Med*. 1993;29:599–604.
26. Perez JM, Josephson L, O'Loughlin T, Hogemann D, Weissleder R. Magnetic relaxation switches capable of sensing molecular interactions. *Nat Biotechnol*. 2002;20:816–820.
27. Weissleder R, Moore A, Mahmood U, Bhorade R, Benveniste H, Chiocca EA, Basilion JP. In vivo magnetic resonance imaging of transgene expression. *Nat Med*. 2000;6:351–355.
28. Lewin M, Carlesso N, Tung CH, Tang XW, Cory D, Scadden DT, Weissleder R. Tat peptide-derivatized magnetic nanoparticles allow in vivo tracking and recovery of progenitor cells. *Nat Biotechnol*. 2000;18: 410–414.
29. Zhu B, Jaffer FA, Ntziachristos V, Weissleder R. Development of a near infrared fluorescence catheter: operating characteristics and feasibility for atherosclerotic plaque detection. *J Phys D Appl Phys*. 2005;38: 2701–2707.
30. Ntziachristos V, Tung CH, Bremer C, Weissleder R. Fluorescence molecular tomography resolves protease activity in vivo. *Nat Med*. 2002; 8:757–760.
31. Sosnovik DE, Schellenberger EA, Nahrendorf M, Novikov MS, Matsui T, Dai G, Reynolds F, Grazette L, Rosenzweig A, Weissleder R, Josephson L. Magnetic resonance imaging of cardiomyocyte apoptosis with a novel magneto-optical nanoparticle. *Magn Reson Med*. 2005;54:718–724.
32. Cunningham CH, Arai T, Yang PC, McConnell MV, Pauly JM, Conolly SM. Positive contrast magnetic resonance imaging of cells labeled with magnetic nanoparticles. *Magn Reson Med*. 2005;53:999–1005.
33. Aikawa E, Farber M, Mendelson K, Padera RF, Aikawa M, Schoen FJ. Human cardiac valve remodeling by activated cells from fetus to adult: implications for postnatal adaptation, pathology and tissue engineering. *Circulation*. 2006;113:1344–1352.
34. Rothman A, Mann D, Behling CA, McGraw M, Seslar S, Shiu P, Zhang L, Kriett JM. Increased expression of endoarterial vascular cell adhesion molecule-1 mRNA in an experimental model of lung transplant rejection: diagnosis by pulmonary arterial biopsy. *Transplantation*. 2003;75: 960–965.
35. Hill PA, Main IW, Atkins RC. ICAM-1 and VCAM-1 in human renal allograft rejection. *Kidney Int*. 1995;47:1383–1391.
36. Tanaka H, Sukhova GK, Libby P. Interaction of the allogeneic state and hypercholesterolemia in arterial lesion formation in experimental cardiac allografts. *Arterioscler Thromb*. 1994;14:734–745.
37. Nakajima H, Sano H, Nishimura T, Yoshida S, Iwamoto I. Role of vascular cell adhesion molecule 1/very late activation antigen 4 and intercellular adhesion molecule 1/lymphocyte function-associated antigen 1 interactions in antigen-induced eosinophil and T cell recruitment into the tissue. *J Exp Med*. 1994;179:1145–1154.
38. Bentley AM, Durham SR, Robinson DS, Menz G, Storz C, Cromwell O, Kay AB, Wardlaw AJ. Expression of endothelial and leukocyte adhesion molecules intracellular adhesion molecule-1, E-selectin, and vascular cell adhesion molecule-1 in the bronchial mucosa in steady-state and allergen-induced asthma. *J Allergy Clin Immunol*. 1993;92:857–868.
39. Alexiou D, Karayiannakis AJ, Syrigos KN, Zbar A, Kremmyda A, Bramis I, Tsigris C. Serum levels of E-selectin, ICAM-1 and VCAM-1 in colorectal cancer patients: correlations with clinicopathological features, patient survival and tumour surgery. *Eur J Cancer*. 2001;37:2392–2397.
40. Maurer CA, Friess H, Kretschmann B, Wildi S, Muller C, Graber H, Schilling M, Buchler MW. Over-expression of ICAM-1, VCAM-1 and ELAM-1 might influence tumor progression in colorectal cancer. *Int J Cancer*. 1998;79:76–81.
41. Aikawa M, Sugiyama S, Hill CC, Voglic SJ, Rabkin E, Fukumoto Y, Schoen FJ, Witztum JL, Libby P. Lipid lowering reduces oxidative stress and endothelial cell activation in rabbit atheroma. *Circulation*. 2002;106: 1390–1396.
42. Verschuren L, Kleemann R, Offerman EH, Szalai AJ, Emeis SJ, Princen HM, Kooistra T. Effect of low dose atorvastatin versus diet-induced cholesterol lowering on atherosclerotic lesion progression and inflammation in apolipoprotein E*3-Leiden transgenic mice. *Arterioscler Thromb Vasc Biol*. 2005;25:161–167.

CLINICAL PERSPECTIVE

Current clinical imaging of atherosclerosis visualizes primarily arterial anatomy or perfusion. However, existing methods do not interrogate the biology of plaques now considered pivotal in the thrombotic complications of atherosclerosis, including acute coronary syndromes and many strokes. This report describes the development and experimental validation of a novel molecular imaging technique that assesses lesion biology by imaging vascular cell adhesion molecule-1. Application of this technique could provide functional information related directly to recruitment of inflammatory cells to atheromata not accessible by classic imaging approaches and add to the identification of plaques likely to cause thrombotic complications.

Noninvasive Vascular Cell Adhesion Molecule-1 Imaging Identifies Inflammatory Activation of Cells in Atherosclerosis

Matthias Nahrendorf, Farouc A. Jaffer, Kimberly A. Kelly, David E. Sosnovik, Elena Aikawa, Peter Libby and Ralph Weissleder

Circulation. 2006;114:1504-1511; originally published online September 25, 2006;
doi: 10.1161/CIRCULATIONAHA.106.646380
Circulation is published by the American Heart Association, 7272 Greenville Avenue, Dallas, TX 75231

Print ISSN: 0009-7322. Online ISSN: 1524-4539